UNIVERSITÀ DEGLI STUDI DI TRIESTE

3-D structure of the crust and uppermost mantle at the junction between the Southeastern Alps and External Dinarides from ambient noise tomography

This is the peer reviewed (post-print) version of the following article:

Original
3-D structure of the crust and uppermost mantle at the junction between the Southeastern Alps and External Dinarides from ambient noise tomography / Guidarelli, M., Aoudia, A., Costa, G.. - In: GEOPHYSICAL JOURNAL INTERNATIONAL. - ISSN 0956-540X. - 211:3(2017), pp. 1509-1523. [10.1093/gji/ggx379]

Availability:
This version is available at: 11368/2916731 since: 2018-02-16T07:36:05Z

Publisher:

Published
DOI:10.1093/gji/ggx379

Terms of use:

Some rights reserved. More details in the PostPrint rights section below.

License:
Digital Rights Management not defined

Publisher copyright

-.-

(Article begins on next page)

19 October 2026

arTs Università degli Studi di Trieste
Archivio della ricerca – postprint

3-D structure of the crust and uppermost mantle at the junction between the Southeastern Alps and External Dinarides from ambient noise tomography

Mariangela Guidarelli,[1,2] Abdelkrim Aoudia[2] and Giovanni Costa[3]

[1] *Istituto Nazionale di Oceanografia e di Geofisica Sperimentale (OGS), I-34010 Trieste, Italy. E-mail: mguidarelli@inogs.it*
[2] *The Abdus Salam International Centre for Theoretical Physics, I-34151 Trieste, Italy*
[3] *Department of Mathematics and Geosciences, University of Trieste, I-34128 Trieste, Italy*

Accepted 2017 September 10

SUMMARY

We use ambient noise tomography to investigate the crust and the uppermost mantle structure beneath the junction between the Southern Alps, the Dinarides and the Po Plain. We obtained Rayleigh wave empirical Green's functions from cross-correlation of vertical component seismic recordings for three years (2010–2012) using stations from networks in Italy, Slovenia, Austria, Croatia, Serbia and Switzerland. We measure group and phase velocity dispersion curves from the reconstructed Rayleigh waves in the period range 5–30 and 8–37 s, respectively, and we invert the surface wave velocities for tomographic images on a grid of $0.1^\circ \times 0.1^\circ$. After the tomography, the group velocities are then inverted to compute the 3-D shear wave velocity model of the crust and the upper mantle beneath the region. Our shear wave velocity model provides the 3-D image of the structure in the region between Northeastern Italy, Slovenia and Austria. The velocity variations at shallow depths correlate with known geological and tectonic domains. We find low velocities below the Po Plain, the northern tip of the Adriatic and the Pannonian Basin, whereas higher velocities characterize the Alpine chain. The vertical cross-sections reveal a clear northward increase of the crustal thickness with a sharp northward dipping of the Moho that coincides at the surface with the leading edge of the Alpine thrust front adjacent to the Friuli Plain in Northeastern Italy. This geometry of the Moho mimics fairly well the shallow north dipping geometry of the decollement inferred from permanent GPS velocity field where high interseismic coupling is reported. From the northern Adriatic domain up to the Idrija right lateral strike-slip fault system beneath Western Slovenia, the crustal thickness is more uniform. Right across Idrija fault, to the northeast, and along its strike, we report a clear change of the physical properties of the crust up to the uppermost mantle as reflected by the lateral distribution of both group and phase velocity anomalies at relevant periods. Idrija fault is therefore interpreted as a subvertical fault sampling the whole crust. Our 3-D velocity model favours crustal thickening with Adria underthrusting the Alps at a shallow angle north of the Friuli Plain where much of the convergence is absorbed and where the destructive 1976 M_s 6.5 thrust Friuli earthquake sequence took place. In Western Slovenia, the deformation is accommodated by strike-slip motion along the Idrija strike-slip fault system where the destructive 1511 M_w 6.9 right lateral strike-slip event occurred.

Key words: Structure of the Earth; Europe; Seismic tomography; Surface waves and free oscillations; Crustal structure.

1 INTRODUCTION

The region investigated in this study is characterized by the junction between the Southern Alps, the External Dinarides and the Po River sedimentary basin (Po Plain): its present structure is the result of complex tectonic processes that are due to the convergence between the Adriatic plate and the European plate (Fig. 1). The area is also characterized by high seismicity (Fig. 1), especially in the Friuli area and Western Slovenia (Aoudia *et al*. 2000; Bajc *et al*. 2001; Fitzko *et al*. 2005; Borghi *et al*. 2009) and transfers up to 3 mm yr^{-1} as inferred from GPS data (e.g. Métois *et al*. 2015). Therefore, a better knowledge of the 3-D distribution of the crustal and upper-mantle

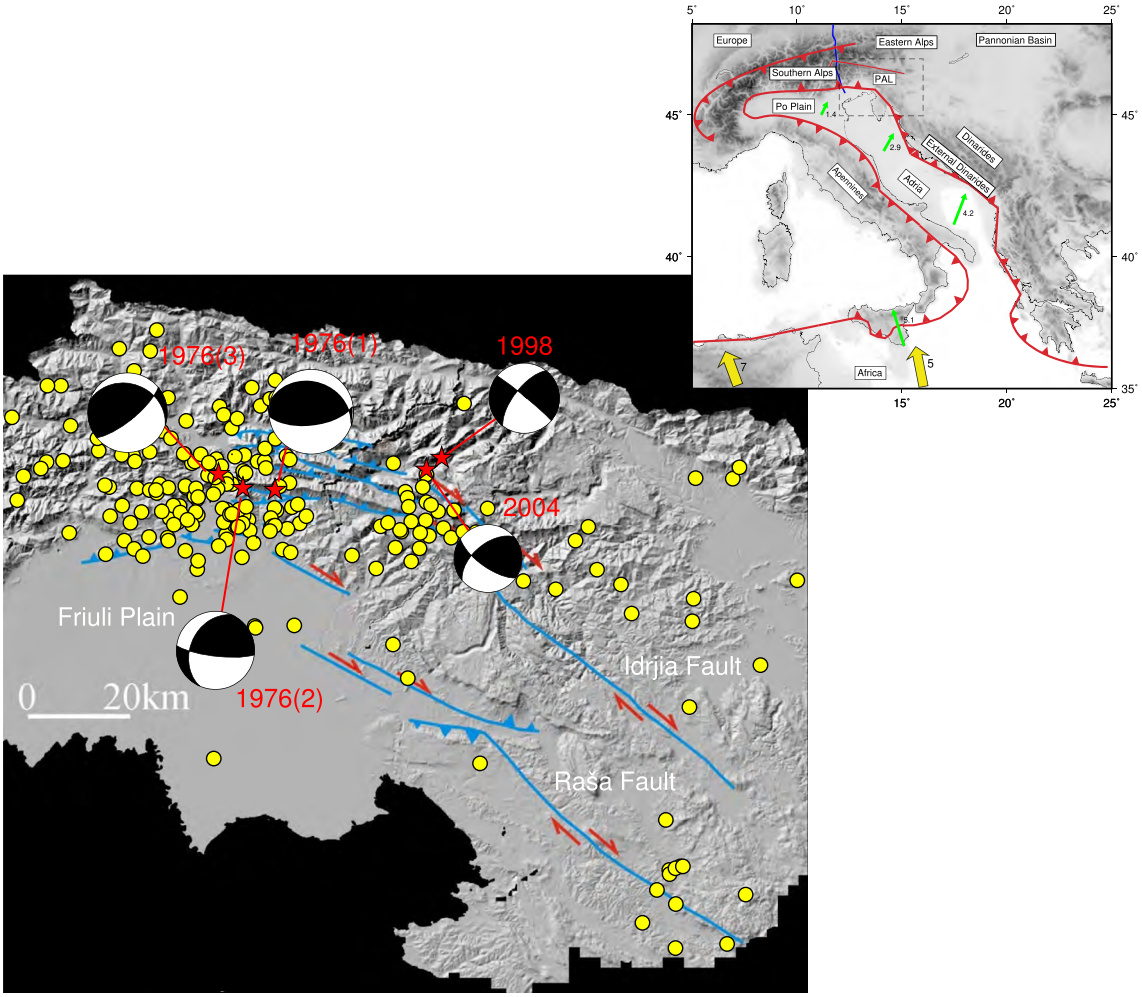

Figure 1. Seismotectonic setting at the junction between the Southeastern Alps and Dinarides (modified from Aoudia 1998). Main active faults and moment tensor focal mechanisms (CMT, http://www.globalcmt.org/) are shown together with 1973–2016 seismicity ($M \geq 3.5$, yellow dots) from National Earthquake Information Center (NEIC, http://neic.usgs.gov). The inset shows a simplified map of the plate boundaries and major tectonic elements of the Italian Peninsula. Yellow arrows show Africa-Europe plate motion predicted by NUVEL-1A (DeMets *et al*. 1994), while green arrows are taken from D'Agostino *et al*. (2008). Numbers on vectors show approximate rates of velocities (in mm yr^{-1}). Blue line: TRANSALP profile (TRANSALP Working Group 2002). Grey rectangle: boundaries of the study area. PAL: Periadriatic Line.

properties is important to improve the understanding of the complex continental collisional processes taking place in this region part of the peri-Adriatic belt.

Despite the availability of a dense seismic network, the number of studies that investigated the lithosphere in the region is limited. The non-uniformity in the geographical distribution of earthquakes in the eastern part of the Southern Alps and the Dinarides, does not allow the use of classic seismic tomography methodologies to reconstruct a 3-D model of seismic velocities in the area. Therefore, to image the lithospheric structure beneath the study region, we used the ambient noise tomography (ANT) methodology. ANT has become an increasingly well-established method to estimate surface wave velocities (group and phase velocities) and therefore map *Vs* at different scales (e.g. Sabra *et al*. 2005; Shapiro *et al*. 2005; Lin *et al*. 2008). The use of ambient noise allows us to measure surface wave dispersion at shorter distances and shorter periods compared to teleseismic surface wave observations that are generally limited to long periods and thus mostly affected by mantle structure. Therefore, surface wave tomography based on cross-correlations of ambient seismic noise can image velocity structures in the crust and the uppermost mantle.

Other studies that made use of ANT to investigate the crustal structure in adjacent areas have recently been published. Li *et al*. (2010a) and (2010b) obtained group velocity maps of Rayleigh and Love waves in the Italian Peninsula, but with a limited coverage and resolution in Northeastern Italy and Slovenia. Behm *et al*. (2016) applied ANT to data from temporary networks in the Eastern Alps and our study region is at the southernmost tip of their tomographic maps.

In this study, we applied the ANT technique to image the crustal velocity structure in northeast Italy and Slovenia. We collected continuous data recorded between 2010 and 2012 from 66 broad-band permanent stations in Italy, Slovenia, Austria, Croatia, Serbia and Switzerland to extract Green's functions from the ambient seismic noise field. We calculated tomographic maps for Rayleigh wave group velocity in the period range 5–30 s and phase velocity in the period range 8–37 s. As a final step, we inverted the Rayleigh wave dispersion curves to obtain the 3-D crustal structure (*S*-wave

velocity) underneath the region that comprises the junction between the Southern Alps, the Dinarides and the Po Plain. With the station distribution in the study region, we were able to provide a more homogeneous sampling over the study region than previous studies and regional seismic tomography using earthquakes.

2 STUDY AREA

The Alps and Dinarides are orogens with different subduction polarities: Adria is the collision upper plate in the Alps, while it is the lower plate in the Dinarides (e.g. Schmid *et al*. 2008, Fig. 1). These three units represent that part of the so-called Adriatic, or Adria, plate which is located south of the Periadriatic Line (PAL). The PAL, also named Insubric Line, is a right-lateral transpressive fault of Oligocene–Neogene age that marks the boundary between the Southern and the Eastern Alps (e.g. Dal Piaz *et al*. 2003). The Southern Alps are a major structural division of the Alpine Chain that overthrust the Adriatic foreland and the Po Plain to the west and the External Dinarides to the east. The Southern Alps are characterized by a dominantly south-vergent fold-and-thrust belt (e.g. Castellarin *et al*. 2006). The area underwent intensive post-collisional back thrusting, since Palaeogene times, which generated the south-vergent structure (Doglioni & Bosellini 1987; Castellarin *et al*. 1992).

The easternmost part of the Southern Alps is characterized by the ENE–NE trend in the Friuli structural belt, dominated by prominent NE–SW trending thrusts, SE-verging folds (Castellarin & Cantelli 2000). The Po Plain is a sedimentary basin filled by the Late Neogene sediments of Alpine and Apenninic origin.

The External Dinarides are a thrust-and-fold belt, part of the Alpine orogenic system; they can be considered as the detached, back thrust and highly deformed upper crust of the Adria during subduction to the NE (e.g. Korbar 2009). The long-lived compressional eastern contact between Adria and Europe has formed and consequently deformed the Dinarides thrust-and-fold belt. The Dinaric area is characterized by dextral subvertical faults, with orientations from NW–SE to NNW–SSE, the most important of which are the Idrija fault and the Raša Fault (Moulin *et al*. 2016, see Fig. 1).

According to Doglioni & Carminati (2002), the European plate is subducted under the Adriatic plate along the whole Alpine arc, while the Adriatic plate is subducted under the Dinarides and Apennines. Lippitsch *et al*. (2003) suggest, instead, the presence of two separate past subduction zones beneath the Western and Eastern Alps, respectively. Brückl *et al*. (2010) support the idea of the subduction of Europe below Adria from north to south and underthrusting of Adria below Pannonian from southwest to northeast.

The kinematics of Adria plate and its interaction with the Alps and Dinarides has been assessed from GPS measurements. Bennet *et al*. (2008) results are consistent with subduction of Adria lithosphere beneath the Dinarides. D'Agostino *et al*. (2008) and Métois *et al*. (2015) suggest that Adria plate rotates in such a way to accommodate Europe-Africa relative motion, moving independently relative to both Europe and Africa. The convergence between Adria and Europe plates being absorbed within the Southeastern Alps, where the Adriatic lithosphere underthrusts beneath the mountain belt (Cheloni *et al*. 2014).

The investigation of the crust in this region was conducted using deep seismic sounding experiments, local scale tomographic studies and some teleseismic tomographic analysis of the upper mantle. For the Friuli region, Bressan *et al*. (1992, 1998) used local earthquakes to obtain a local 3-D *P*-wave velocity model in the area that revealed strong lateral and deep heterogeneities in the upper crust, related to the presence of a southward-verging thrusted wedge of basement. Gentile *et al*. (2000) performed a 3-D joint inversion for hypocentres and velocity structure in the Friuli area and they found again that the upper crust is characterized by strong heterogeneities, with a high-velocity body in the central part of the area at about 6 km depth; they also found high V_P/Vs values associated with highly fractured zones related to the main faulting pattern. Similarly, the inversion for hypocentres and velocity structure in Slovenia (Michelini *et al*. 1998) revealed a high *P*-wave velocity body in the western part of Slovenia between 3 and 15 km depth. Stipčević *et al*. (2011) investigated the crustal and uppermost mantle structure using receiver functions for some locations: in the NW Dinarides they found a Moho depth of about 40 km.

A series of controlled source seismic experiments were conducted in the last decade in order to constrain the structure of the crust and upper mantle in central Europe. Several studies provide information about the crust beneath the junction between the Eastern Alps, the Southern Alps and the Dinarides. In 2002, the TRANSALP programme (TRANSALP Working Group 2002) produced the first seismic profiles for the Eastern and Southern Alps (from Germany to Italy) from seismic reflection data, revealing the main double vergent structure of the Alps. The resulting models reveal that the European Moho is dipping south at an angle of 7°, whereas the Adria plate is dipping north at a shallower angle. Bleibinhaus & Gebrande (2006) proposed *P*-wave velocity models obtained from active source traveltime tomography that show significantly higher *P*-wave velocities in the Adriatic crust (stronger, more rigid crust) than the European crust. Their findings suggest the existence of an *S*-directed subduction of the European plate and the presence of a deep thrust fault in the Southern Alps at about 20–25 km. Brückl *et al*. (2007) showed that the European Moho dips to the south and reaches a maximum depth of 47 km below the transition from the Eastern to the Southern Alps. The Adriatic Moho continues further south at a significantly shallower depth, supporting the idea of southward subduction of the European lithosphere below the Adriatic. Brückl *et al*. (2010) explained the results of controlled source seismic experiments with the subduction of Europe below Adria from north to south and underthrusting of Adria below Pannonian from southwest to northeast. They also suggest that the active tectonic processes at surface are strongly related to the Moho fragmentation, with a thickening of the Adriatic crust under the Southern Alps.

Behm *et al*. (2007) and Behm (2009) interpreted 3-D seismic wide-angle reflection and refraction data to obtain V_P and Vs models within the longitude range between 14° and 19° E. Their results suggest a fragmentation of the crust in the Eastern Alps into three main blocks, with different Moho depths and dipping characteristics.

Vosteen *et al*. (2003) from petrophysical heat-flow data showed that the Alpine roots are characterized by significantly higher temperatures compared to the Adriatic. The lower temperatures and the high velocities of the Adriatic crust (Bleibinhaus & Gebrande 2006) also indicate a stronger, more rigid crust than on the European side.

Lippitsch *et al*. (2003) from high-resolution teleseismic tomography found a high-velocity anomaly in the eastern Alps that can be traced down to about 300 km, with a clear connection to Adriatic lower lithosphere that dips to the northeast and is subducted beneath the European plate. Mitterbauer *et al*. (2011) obtained tomographic images of the upper mantle from teleseismic waveforms. They revealed a shallow slab below the Eastern Alps down to about 250 km, interpreted as European lower lithosphere

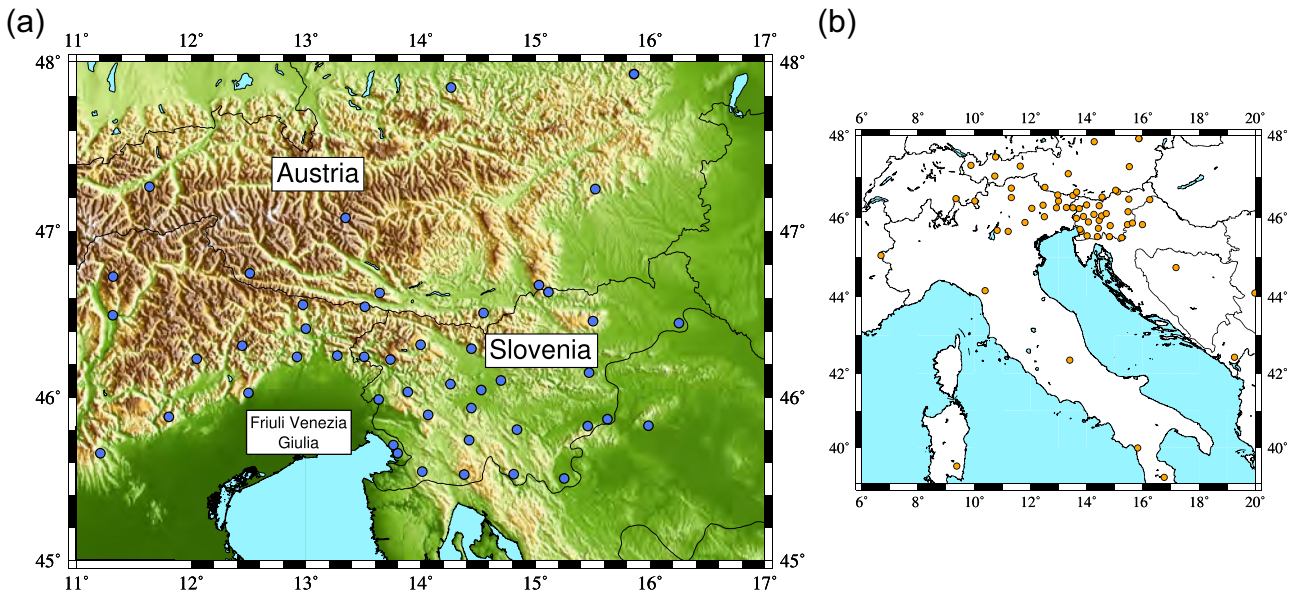

Figure 2. (a) Topographic map of the Eastern-Southern Alps region with the distribution of the broad-band stations used in this study inside the area (blue dots). (b) Map with the full set of the stations used in this study.

detached from the crust subducted during collision between Adria and Europe.

3 DATA AND INVERSION

3.1 Data

We collected continuous broad-band vertical component seismic data recorded between 2010 and 2012 by 66 stations in Italy, Slovenia, Austria, Croatia, Serbia and Switzerland from the following sources: Central Eastern European Earthquake and Research Network (Costa *et al*. 2010; Bragato *et al*. 2014), Serbian Network of Seismic Stations and Switzerland Seismological Network (Swiss Seismological Service 2015). The stations used in this study are plotted in Fig. 2. We used data also from some stations of the Mediterranean Very Broad-band Seismographic Network located outside of the study region in order to increase the aperture of the station network and therefore extend the period range. Given the distribution of the seismic stations used and the maximum distance between station couples (a reliable dispersion measurement at any period requires an interstation spacing of at least three wavelengths, as stated by Bensen *et al*. 2007), we decided to focus our ambient noise tomographic analysis in the period range 2–40 s, restricting the resolving power of our data set to the crust and the uppermost mantle.

3.2 Processing and dispersion analysis

A detailed discussion of cross-correlation processing for ambient seismic noise is given by Bensen *et al*. (2007) and our processing scheme follows that approach. We used continuous vertical component seismograms to obtain two-station cross-correlation functions on one-day long waveforms to estimate Rayleigh wave Green's functions. We first prepared data for each station removing the instrument response, the mean and the trend from one-day data files; then we bandpass filtered the signals (2–40 s), applied the running-absolute-mean normalization (Bensen *et al*. 2007) prior to cross-correlation, and finally a spectral whitening. Time-domain normalization is a procedure for reducing the effect on the cross-correlations of earthquakes, instrumental irregularities and non-stationary noise sources near to stations.

After the time-series has been processed for each day, we then computed daily cross-correlations between all station pairs and then stack the results. We cross-correlated daily time-series for all the station pairs and then stacked the daily cross-correlations over the period of about 2 yr; this time span is sufficiently long to guarantee that the ambient noise is randomly distributed (Stehly *et al*. 2006). We also cut the cross-correlation function into positive and negative time lags and then add the two lags to build an average cross-correlation in order to reduce the effects of inhomogeneity of the seismic noise source distribution and enhance the signal-to-noise ratio (SNR; Yang & Ritzwoller 2008). Fig. 3 shows an example of a record section of cross-correlations with respect to the common station TRI. This figure shows that a variety of azimuths produce visible signals and a clear moveout of the prominent signals. Prominent signals appear at both positive and negative correlation lag times on each stacked cross-correlation, which represent waves traveling in opposite directions between stations.

We evaluated the quality of the cross-correlations quantitatively according to the criteria suggested by Bensen *et al*. (2007). We first calculated the SNR for each interstation cross-correlation. SNR is defined as the ratio of the peak amplitude within the time window containing the Green's function to the root-mean-square of noise trailing the signal arrival window. Then, we rejected cross-correlations if their SNR < 10. Then, we applied the repeatability criterion according to which for a measurement to be accepted, it needs to be repeatable in the sense that measurements obtained at different times should be similar. For each station pair, we considered several overlapping 3-month stacks and computed the SNR for each of them. The cross-correlation is retained if more than 10 stacks have an SNR > 10. For those station pairs, we measured the dispersion on all sequential 3-month stacks and then computed the standard deviation of the measurements to estimate the

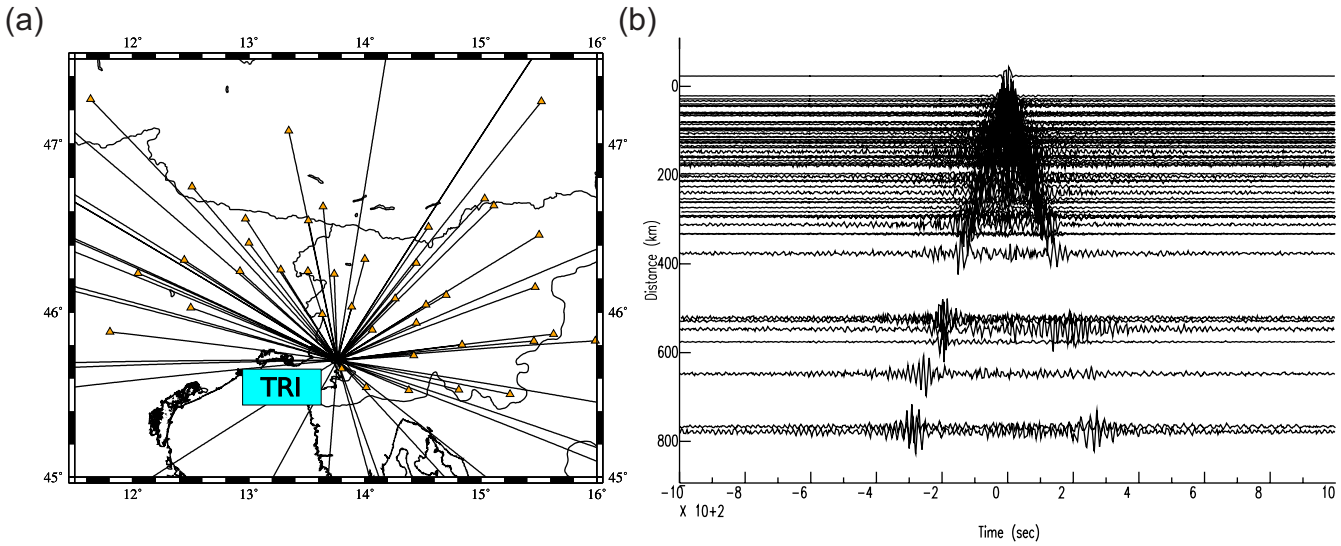

Figure 3. Example of cross-correlations obtained from 2 yr of data between station TRI and all other stations (a) used in this study (2–40 s period) plotted as a function of distance (b).

uncertainties. After the application of quality control criteria, we remained with 2067 reliable cross-correlations.

3.3 Group and phase velocity measurement

For each accepted station pair cross-correlation, the group and phase velocity dispersion curves were measured using traditional frequency–time analysis (FTAN); a detailed description of the methodology can be found in Levshin & Ritzwoller (2001). We resolved the phase ambiguity common to all phase velocity measurements using average phase velocities as the reference (e.g. Farina 2006).

We measured both group and phase velocities to better constrain the shear wave velocity model in the study area. Even if the group velocities are conventionally easier to measure, Lin *et al*. (2008) pointed out that phase velocities have several advantages among which smaller uncertainty with respect to the group velocities and a deeper sensitivity kernel, therefore phase velocities sample deeper velocity structures.

We computed Rayleigh wave group velocity for 2067 interstation paths, in the period range 5–30 s and phase velocities in the period range 8–37 s. According to Bensen *et al*. (2007), the dispersion measurements from cross-correlations are reliable only for distances at least three wavelengths. For this reason, each dispersion curve is accepted only up to a maximum cut-off period of above $d/12$ in seconds, where d is the distance. A recent study showed how surface wave phase velocity dispersion curves are reliable for distances up to only one wavelength (Luo *et al*. 2015). For this reason, we slightly relaxed the three-wavelength criterion for phase velocities, reaching a maximum period of 37 s, but never considering less than two wavelengths. As an additional criterion to select the most reliable dispersion measurements for tomography, we required that measurements must cohere with one another across the data set; coherence relates to the mutual agreement of measurements that cross the same region and it will be verified during tomography, trying to fit the data with smooth tomographic maps. As an example of group and phase velocity measurements, Fig. 4 shows a cross-correlation between a couple of stations, and the resulting dispersion curves.

4 SURFACE WAVE TOMOGRAPHY

We constructed group and phase velocity maps from the estimated Rayleigh waves Green's functions at periods from 5 to 30 and 8 to 37 s, respectively. We used the group and phase dispersion measurements to invert for tomographic maps on a $0.1^\circ \times 0.1^\circ$ grid across the region using the method of Yanovskaja & Ditmar (1990). The method does not require any *a priori* parametrization of the basis functions but is based on the assumption of the smoothness of the velocity function depending on a regularization parameter. According to Yanovskaya *et al*. (1998), the regularization parameter was chosen so that the output velocities are within the range defined by the observed dispersion curves and the final unaccounted traveltime residuals are distributed randomly. The density of paths, the azimuthal coverage and the average paths length control the spatial resolution of the results. According to the method described by Yanovskaya (1997), information of the resolution is summarized by a single scalar at each node, called the horizontal spatial resolution. Examples of resulting tomography maps are shown in Figs 5 and 6, with velocities represented as percentage variation with respect to the mean velocity. The tomography maps at 5, 10, 16, 20 25 and 30 s for group velocity and at 8, 12, 16, 20, 30 and 37, s for phase velocity are shown. The plots are arranged in order of increasing period in order to represent the increasing penetration into the Earth. Different velocity scales are used for different periods to take into account the increasing of velocity at higher periods. The black contour lines plotted on each map represent the isolines of the estimated horizontal spatial resolution at each period. The lateral resolution of group and phase velocities is about 40 km in many parts of the study area and for periods until 30 s, it degrades toward the margins of the map where the paths are few and not crossing each other. The ray path coverage at each period is also plotted in the inset; except for the shorter periods (5–8 s), the path coverage is quite good over the whole study area.

4.1 Rayleigh waves group and phase velocity maps

Surface waves at different periods are sensitive to structures at different depths. To guide the qualitative interpretation of tomographic maps, Fig. 7 shows the sensitivity kernels for Rayleigh wave group

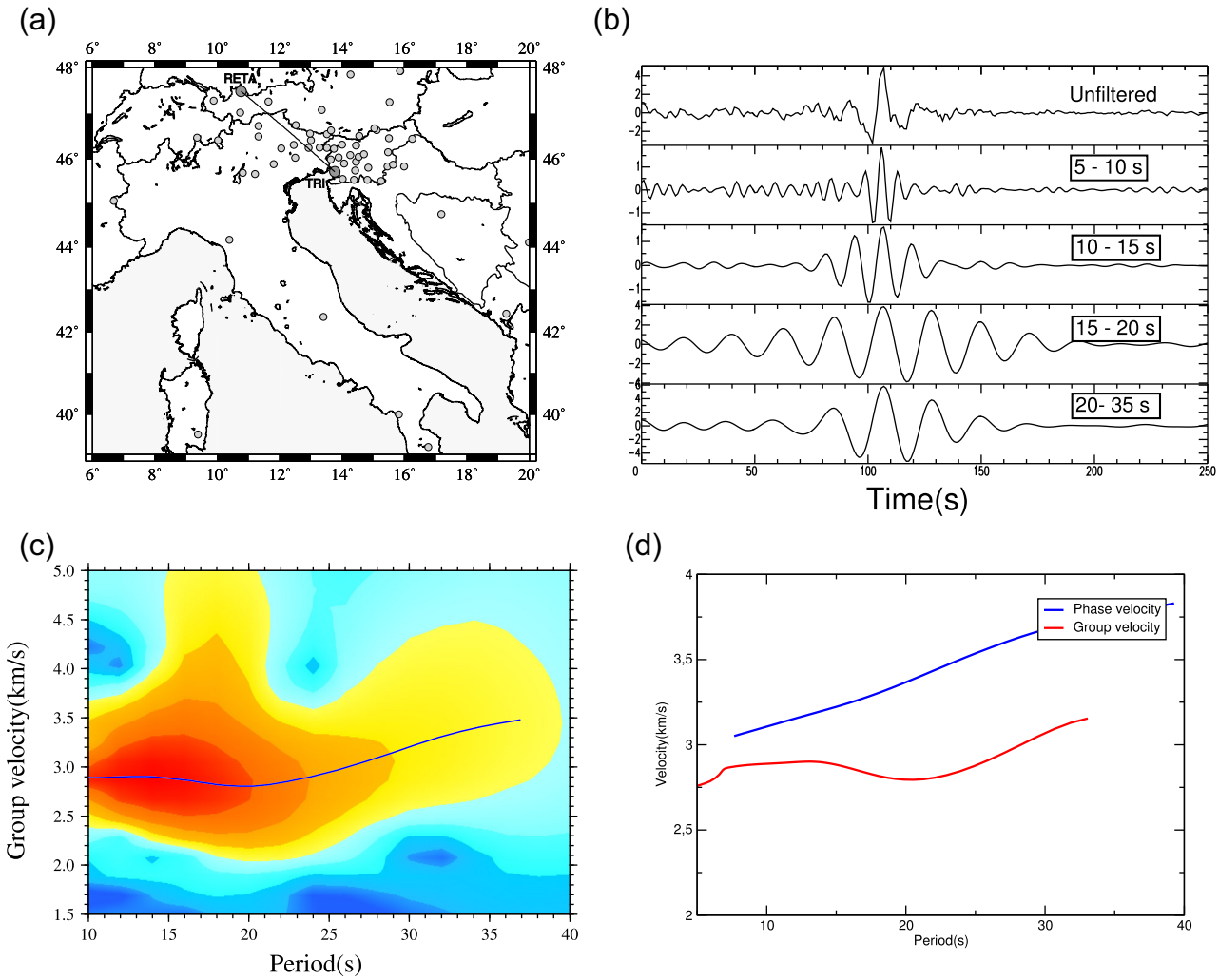

Figure 4. Example of dispersion measurement. (a) Ray paths between station TRI and RETA. (b) Cross-correlation for station pair TRI-RETA bandpass filtered at different periods. (c) FTAN diagram showing the group velocity dispersion curve for the path TRI-RETA. (d) Group and phase velocity dispersion curves measured for the path TRI-RETA.

and phase velocities computed using the AK135 model. The depth of maximum sensitivity is about one-third of a wavelength. At the short-period end of this study (5–10 s), group velocities are strongly affected by shallow crustal structure, with short-period low-velocity anomalies being a good indicator of sedimentary basins. At the intermediate periods (15–25 s), group velocities are sensitive to middle and lower crustal shear velocities. At periods longer than 30 s, Rayleigh waves are influenced by the Moho depth and the shear velocities in the lower crust and uppermost mantle, where *Vs* exhibits a significant increase. Thanks to those large velocity contrasts across the Moho, the group and phase velocities after 30 s period should vary approximately inversely with crustal thickness, with high velocities in regions with thin crust and low velocities in regions with thick crust. In general, at any given period, phase velocity is sensitive to structure at depths greater than group velocity. The average group velocities of our tomographic maps, that vary from 2.77 to 3.14 km s^{-1} in the period 5–30 s, are consistent with the values presented by Li *et al*. (2010a,b), which are however characterized by a lower spatial resolution.

In Figs 5 and 6, we clearly recognize at short periods the signature of the main shallow geological features. A low-velocity anomaly in group velocity map at 5 s can be associated to the Po Plain, characterized by Plio-Pleistocene sediments, that may reach an average thickness of 7–8 km (Molinari *et al*. 2015), and the Adria microplate. The anomaly clearly marks the boundary between Adria and Southern Alps to the north, and between Adria and External Dinarides to the east, indicating that Istria peninsula belongs to the Adria foreland. The slow anomaly in the eastern part of the map appears to be associated with the region where Southern Alps, Dinarides and Pannonian Basin intersect. The lowest velocity indicates the presence of the Tertiary cover at the periphery of the Pannonian Basin that can reach a thickness of 6 km. The low velocity propagates towards west until the area that corresponds to the Ljubljana basin. Higher velocities seem to characterize southwest Slovenia and in general the northernmost Dinarides. The highest velocity anomaly is located in correspondence of the Southern Alps and their boundary with the Eastern Alps. Behm *et al*. (2016) also found increasing group velocities moving northward from the northwestern corner of Slovenia, with values from 2.7 to 2.9 km s^{-1} across the PAL. Group velocity map at 10 s and phase velocity map at 8 s show similar characteristics and clearly outline the boundaries between Adria plate (low velocities), Southern and Eastern Alps (very high velocities), Dinarides and the periphery of the Pannonian Basin (low velocity).

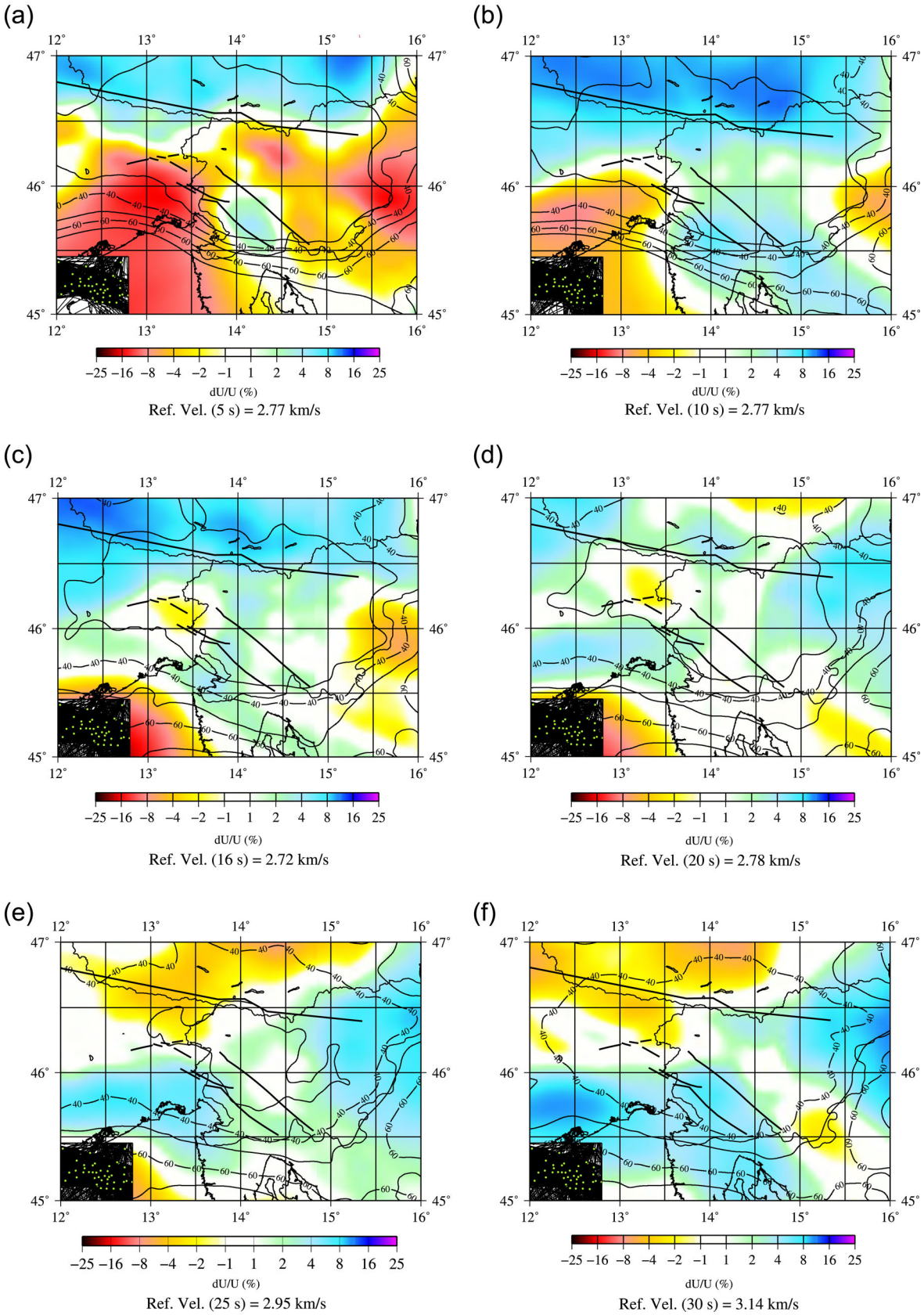

Figure 5. (a)–(f) Maps of group velocities resulting from ambient noise tomography at the indicated periods (s) in percentile deviation from the average velocity (Ref. Vel.). The black contour lines represent the horizontal spatial resolution in kilometres. The ray coverage for each period is also shown (insets). Black lines are the main lineaments as traced in Fig. 1.

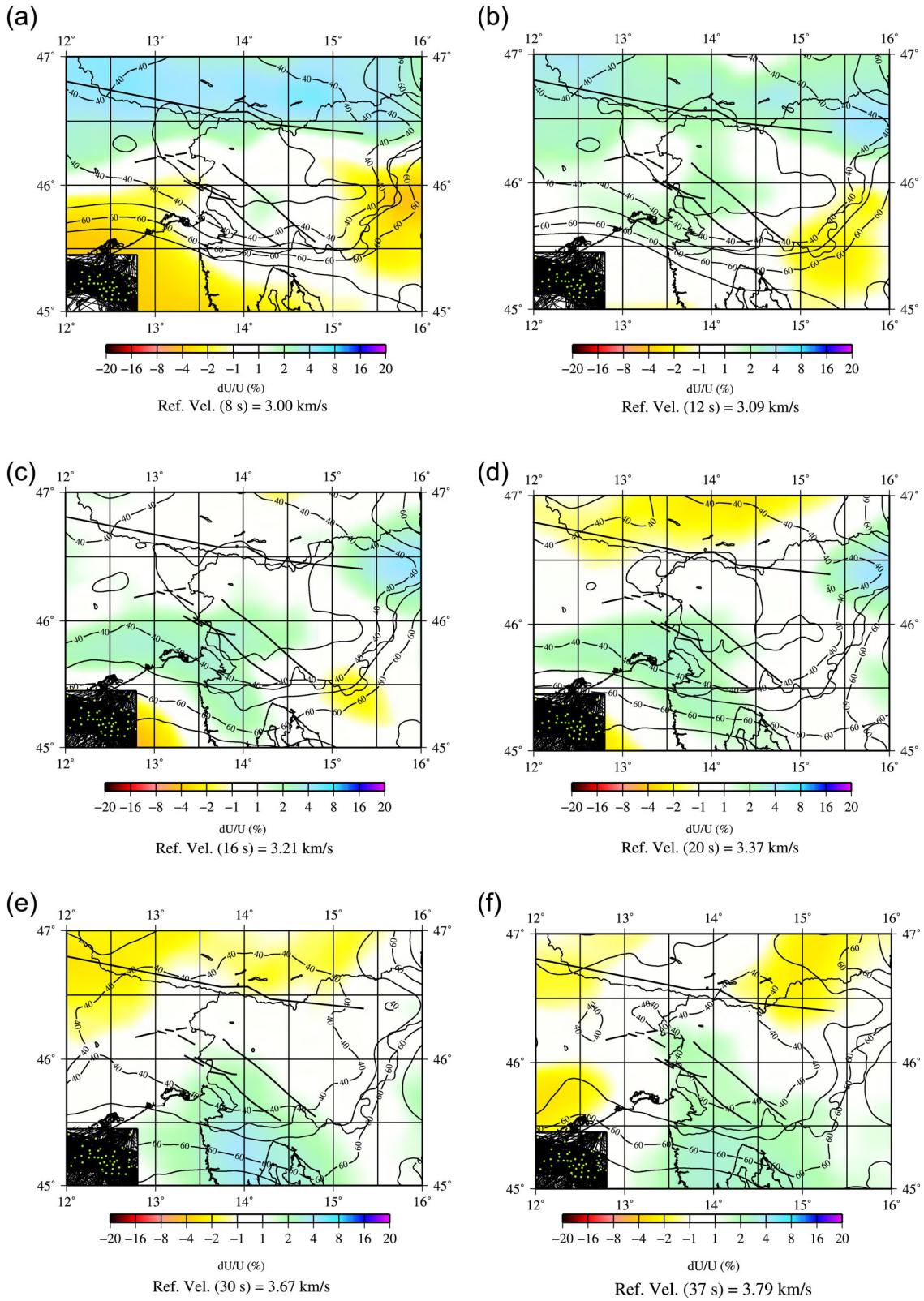

Figure 6. (a)–(f) Maps of phase velocities resulting from ambient noise tomography at the indicated periods (s) in percentile deviation from the average velocity (Ref. Vel.). The black contour lines represent the horizontal spatial resolution in kilometres. The ray coverage for each period is also shown (insets). Black lines are the main lineaments as traced in Fig. 1.

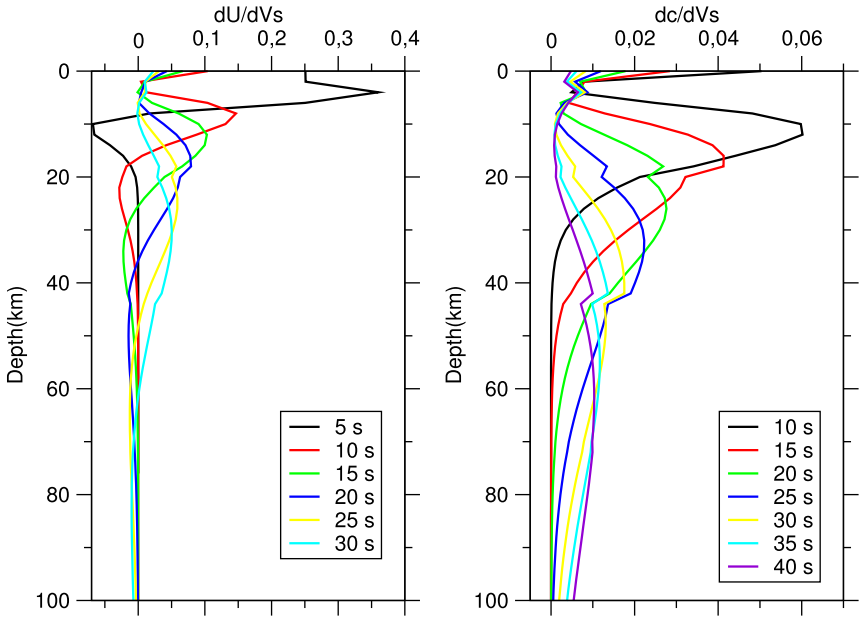

Figure 7. Depth sensitivity kernels of group (left) and phase (right) velocity versus shear wave velocity computed with the AK135 model.

At intermediate periods, 16 s for group velocity and 12 s for phase velocity, low-velocity anomalies reduce. Sensibly lower group velocities persist in the Adria microplate and high velocities in correspondence of the Alpine chain. At the junction between Southern Alps, Dinarides and Adria, the distribution of velocities appears more irregular, indicating a more complicated structure in middle crust. At periods sensitive to lower crust, group (20 s) and phase velocities (16–20 s) indicate the transition from crust to upper mantle. Group velocity maps delineate a discontinuous distribution of velocities, while phase maps are more regular, with lower than average velocities beneath the Alps and higher velocities at the northern tip of the Adriatic microplate and the periphery of the Pannonian Basin. From 25 s, tomographic maps reflect the velocity contrasts across the Moho and therefore correlate with crustal thickness in the Alps, with deep crustal roots, and the surrounding basins. Group velocities at 30 s delineate a discontinuity in the structure of the Dinarides at depths relative to lower crust/Moho that emerges from phase maps also. Such discontinuity seems to support the hypothesis of fragmentation of the crust and uppermost mantle into Adriatic, Europe and Pannonian plates, as proposed by Behm (2009), Brückl *et al*. (2010) and Mitterbauer *et al*. (2011).

5 INVERSION FOR 3-D SHEAR WAVE VELOCITY STRUCTURE

More detailed interpretation of group and phase velocity maps requires an inversion to determine the *Vs* structure of the crust and uppermost mantle. The group and phase velocity maps from ANT obtained in this study provide unprecedented constraints on crust and upper-mantle properties beneath the study region. To quantify our results in terms of *Vs*, we constructed dispersion curves for each grid node of our group and phase tomographic maps, from 5 to 30 s in group velocity and from 8 to 37 s in phase velocity. We then inverted together phase and group velocity dispersion curves to obtain a 1-D isotropic *Vs* model for each node.

The inversion for the isotropic shear wave velocity structure was carried out using a linearized least-squares inversion scheme (Herrmann 2013). Our parametrization assumed a 1-D model with layer thicknesses of 1 km in the upper 6 km, 2 km from 6 to 60 km and 5 km from 60 to 100 km depth. We run the inversion to a depth of 100 km to avoid forcing structure to artificially shallow depths even if at that depth we are at the limit of resolution of our data set, as we can see from the sensitivity kernels in Fig. 7. The linearized inversion technique shows some dependence on the initial model. To account for this dependence and non-uniqueness, we repeated the inversion using 60 different starting models and five damping factors (the two parameters that mostly influence the inversion results) with a strategy similar to that adopted by Julià *et al*. (2005), Caldwell *et al*. (2009) and Rapine *et al*. (2003). The starting models were defined within the velocity values obtained by previous studies in the area (e.g. Bressan *et al*. 1992; Behm *et al*. 2007; Michelini *et al*. 1998; Farina 2006; Brückl *et al*. 2007). The final *S*-wave velocity structure is the average of the inversion solutions. The standard deviation of the family of the final models is 0.03–0.20 km s^{-1} depending on depth.

With the ensemble of 1-D shear wave velocity profiles determined for each node of the grid in the study area, we can assemble 3-D models interpolating from the spatial grid. Fig. 8 shows the shear wave velocity model at depths of 4, 14, 25 and 40 km, displayed using an absolute velocity scale. The well-resolved areas in these maps at each depth depend on the resolution of surface wave velocities at periods whose sensitivity is maximum at that depth. The structures in the resulting 3-D shear wave velocity model are similar to those observed in the group and phase velocity maps.

The 4 km deep section displayed in Fig. 8 shows the uppermost part of the crust, with *Vs* velocities ranging from 2.7 to 3.3 km s^{-1}, the lowest values typical of unconsolidated sediments in the Po Plain, characterized by Plio-Pleistocene sediments and the Tertiary cover at the periphery of the Pannonian Basin in the eastern part of the map. The distribution of shear wave velocities seem to mark the boundary between Southern Alps and Eastern Alps (PAL): lower velocity in the Southalpine Mesozoic and Tertiary units and higher velocity in the Austro-Alpine units which consist of the Palaeozoic crystalline basement and several Mesozoic cover sequences. The shallow velocity distribution in Slovenia is consistent with that

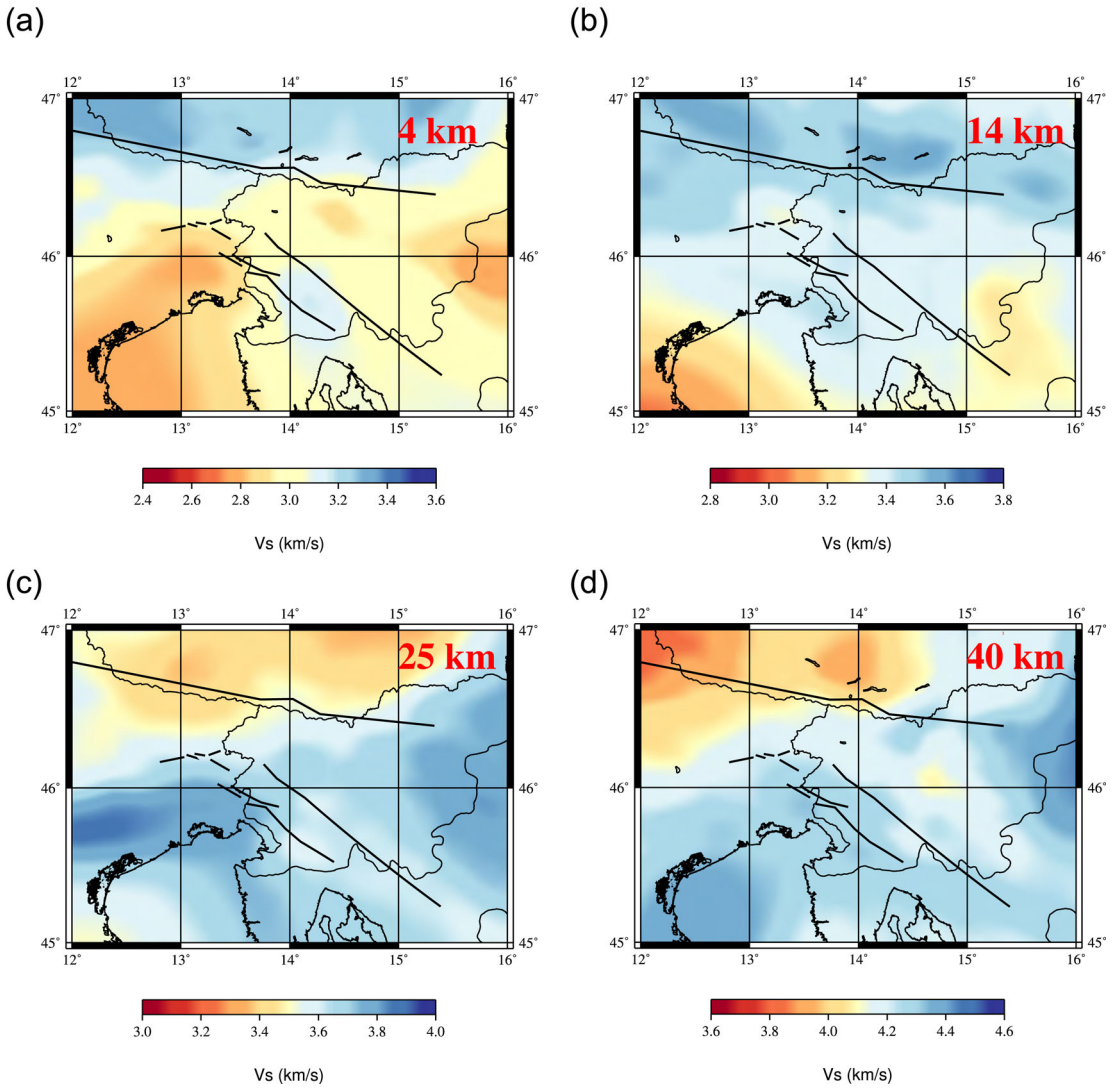

Figure 8. Maps of the shear wave velocity model obtained after inversion of local group and phase velocity dispersion curves at depths: 4, 14, 25 and 40 km. The colour scale changes with depth. Black lines are the main lineaments as traced in Fig. 1.

obtained by Behm *et al*. (2007), with higher velocities in the External Dinarides west of the Idrjia Fault, compared to central and eastern Slovenia. At depths corresponding to middle crust (14 km) lower velocities characterize the SE corner of the study region (Po Plain and Adriatic plate); lower V_P velocities in this area were also found by Dihel *et al*. (2009) from local body wave tomography. *Vs* values of 3.5–3.6 km s^{-1} are found beneath the Alps, with slightly higher velocities north of the PAL. At 25 km depth, corresponding to mid-lower crust, we start seeing reverse velocity anomalies with respect to the upper-middle crust: reduced velocities are mainly associated with the crustal roots of the Alps, while increased velocities likely correlate with upper-mantle velocities of the Adriatic plate. The same trend is visible in the velocity models proposed by Dihel *et al*. (2009) and Di Stefano *et al*. (2009). The distribution of *Vs* across the Alps seems to have no correlation with the PAL, suggesting that the boundary between the Southern and the Eastern Alps is confined in the upper crust. At 40 km depth, the distribution of *Vs* anomalies is correlated with Moho depth. *Vs* values typical of lower crust (3.6–3.9 km s^{-1}) are still present beneath the Alpine chain, while upper-mantle velocities (4.3–4.45 km s^{-1}) are revealed beneath the Adria plate and the eastern part of the map. The composite distribution of velocities at 25 and 40 km in central Slovenia may reflect the existence of a transition zone from the Adria microplate to the Pannonian plate, as hypothesized by Brückl *et al*. (2010). From the *S*-wave velocity models, we could also provide a Moho map (Fig. 9). We place the Moho where the shear wave velocities are close to or exceed the value of 4.3 km s^{-1} (e.g. Christensen & Mooney 1995). Our models result in Moho depths between 35 and 46 km. Crustal thickness increases from south to north, moving from the Adria Plate towards the Southern Alps. Thick crust characterizes also the central part of Slovenia in correspondence of the central Dinarides, where according to Brückl *et al*. (2010), there exists a transition from the thicker Dinaric crust and the thinner Pannonian crust, characterized by complex tectonic interactions. Our Moho map agrees in general with Moho maps computed at a larger scale (e.g. Behm *et al*. 2007; Grad *et al*. 2009; Tesauro *et al*. 2008) and provides more info as our resolving power in the study region is higher.

Figs 10 and 11 show eight cross-sections across different paths in the central part of the study region imaging therefore the interactions between the Adriatic microplate, the Southern Alps and the external Dinarides. The most significant features visible in the

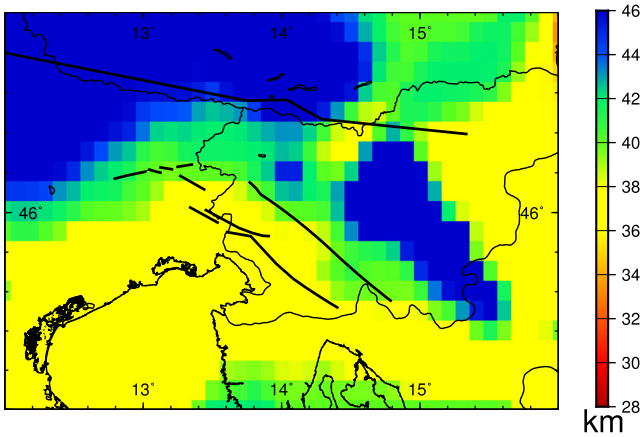

Figure 9. Map with Moho depth values obtained in this study. We place the Moho where the shear wave velocities are close to or exceed the value of 4.3 km s^{-1}. Black lines are the main lineaments as traced in Fig. 1.

cross-sections are represented by the geometry of both the upper crust–lower crust transition and the Moho. A common feature of the sections is the correlation between deeper Moho and higher elevation in the Southern Alps.

In Fig. 10, profile AA′ crosses the Idrjia and Raša faults from the Adriatic in the Southwest to central Slovenia in the northeast: low velocities characterize the upper crust especially in correspondence of the Adriatic and towards the Pannonian Basin. Higher velocities (4.5–4.6 km s^{-1}) are found in the uppermost mantle of the Adria microplate, compared to the Dinarides (4.3–4.4 km s^{-1}); this is consistent with the results of Šumanovac & Dudjak (2016) that explain the high-velocity anomaly as a signature of the Adriatic lithosphere sinking beneath the Dinarides. Profile BB′ crosses profile AA′ and runs parallel to the Idrjia and Raša faults: the profile appears quite uniform in this direction. The cross-section along the Southern Alps (CC′) runs from west to east and shows shear velocities between 3.2 and 3.5 km s^{-1}, typical of the upper crust, in the depth range 10–30 km. In correspondence to the Southern Alps, the first 5 km of the crust show velocities 10–15 per cents lower than the crust beneath the Eastern Alps. From the west end of the CC′ section, it is clear that the Moho rises towards east, beneath the Southern Alps. This section extends parallel to the easternmost part of the Alp02 profile (Brückl *et al*. 2007). In Fig. 10 (section CC′), we sketched the top of the Adriatic mantle and the hypothetical boundary between the European and Adriatic plate as suggested by Brückl *et al*. (2007) along the ALP02 profile. The uplift of the Adriatic mantle is consistent with the trend of the Moho in our cross-section. The jump in the Moho depth is located by Brückl *et al*. (2007) in correspondence to the transition from the Alpine domain to the Pannonian domain, and explained as crustal thinning due to tectonic escape from the Alpine collision area. The transition between European and Adriatic plates at crustal depths is not resolved in our model, but the crustal thickening and a deeper European mantle can be inferred from our section. Section DD′ covers the southernmost part of the path of the Alp01 profile (Brückl *et al*. 2007) and the ALPASS1 profile (Behm *et al*. 2016). Like in Behm *et al*. (2016), we evidence a thickening of a low-velocity layer near the surface south of Eastern Alps. The crustal thickness is maximum beneath Eastern Alps near the PAL, and Moho depth gently increases towards the south. At the end of the profile, higher velocities (4.5–4.6 km s^{-1}) mark the Adriatic mantle. The trend exhibited by section DD′ is coherent with the Alp01 model proposed by Brückl *et al*. (2007), and therefore with a south-dipping European lithosphere and a gently north-dipping Adriatic Moho. Like in CC′ profile, we are not able to resolve the transition between Europe and Adria within the crust; the evident feature is the presence of upper mid-crustal velocities at depth beneath Eastern Alps.

In Fig. 11, the five cross-sections have in common the starting point located in the Adriatic Sea, which is associated with low velocities down to ∼10 km, likely caused by the continuation of the sedimentary pile from the Po Basin, and a crustal thickness of ∼36 km. The five profiles sample the plate boundary between the Adriatic domain and the European plate extending laterally from the Dinarides in the east up to the Southern Alps in the west. Moving westwards from profile OA to profile OE, we can observe in correspondence to the PAL, or transition from Southern Alps to Eastern Alps: (1) an increase of the shear velocities in the first 10 km of the crust that can be likely associated with a reduction of the sedimentary cover; (2) upper crustal velocities that reach depths down to ∼30 km; (3) increase of crustal thickness; (4) deepening of the Moho. In Fig. 11 (section OE), we sketched the trend of the Adriatic and European crust as inferred along the TRANSALP profile (TRANSALP Working Group 2002). Even if the hypothetical transition between the two plates is not resolved in our velocity model, the trend of the lower crust and Moho is coherent with the biverging character of the Alps: the European plate dipping south underneath the Adriatic plate, which is dipping north with a lesser inclination. The inclination of the Adriatic plate seems even gentler in sections OB, OC and OD, where the signature of the dipping European plate is no more visible. Our results are in agreement with the seismic images obtained by the TRANSALP Working Group (2002) that revealed a thickened crust related to the back thrust and indentation of the Adriatic lithosphere underneath the Alps. This supports the idea that active convergence between Europe and Adria is associated with thickening of the crust, caused by the continued indentation of the Adriatic microplate to the north under the Southern Alps (Brückl *et al*. 2010). Specifically on sections OD and OE, the geometry of the Moho mimics fairly well the geometry of the decollement right above it inferred by Cheloni *et al*. (2014) from GPS data set and that is also in good agreement with the faulting geometry of the 1976 Friuli earthquake (Aoudia *et al*. 2000). On the Dinaric side in Western Slovenia the sharp change, striking NW–SE, within both group and phase velocity maps reveals the high dip angle and the lithospheric nature of the Idrija right lateral fault system mapped at the surface. This has serious implications on earthquake hazard as already highlighted by the occurrence of a magnitude 6.9 earthquake in 1511 (e.g. Fitzko *et al*. 2005; Moulin *et al*. 2016) along one of the fault segments of the Idrija fault system. Furthermore, a clear change of the physical properties within the crust across the Idrija fault system as revealed by the tomographic maps implies a sizeable lateral variation within the rigidity that needs to be accounted for in any model investigating the mechanics of the deformation in the region. On the Alpine side in Eastern Italy, the sudden bending of the Adriatic crust coincides with the leading edge of the mountain front at the surface, mimicking both the topography along strike and the geometry of the 1976 Friuli earthquake shallow dipping fault (Aoudia *et al.* 2000) towards its easternmost part.

6 CONCLUSIONS

A new, 3-D shear wave velocity model for the crust and the uppermost mantle of the region that comprises the Southern Alps, the External Dinarides, the Po Plain and the northern Adria microplate

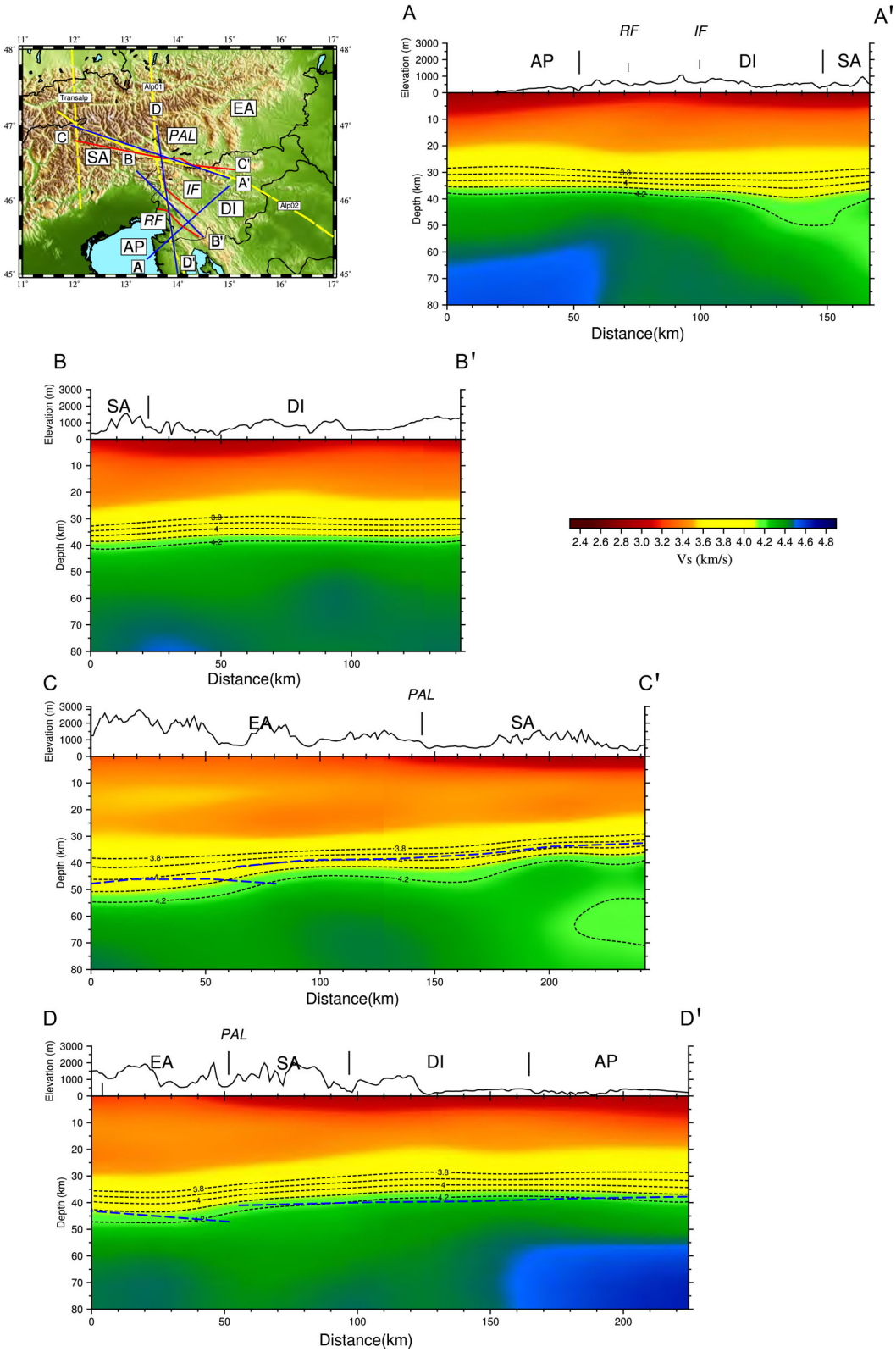

Figure 10. Vertical sections through the 3-D shear wave velocity model along the profiles showed in the map: AA′, BB′, CC′ and DD′. The black dashed lines show the isolines of velocity from 3.8 to 4.2 km s^{-1}. SA Southern Alps; PAL Periadriatic Line; EA Eastern Alps; IF Idrjia Fault; RF Raša Fault; DI Dinarides; AP Adriatic Plate; EA Eastern Alps. The TRANSALP, ALP01 and ALP02 profiles are also plotted (yellow dashed lines). Section CC′ and DD′: (blue dashed lines) depth to the top of the mantle, for ALP02 and ALP01 models respectively (Brückl *et al*. 2007).

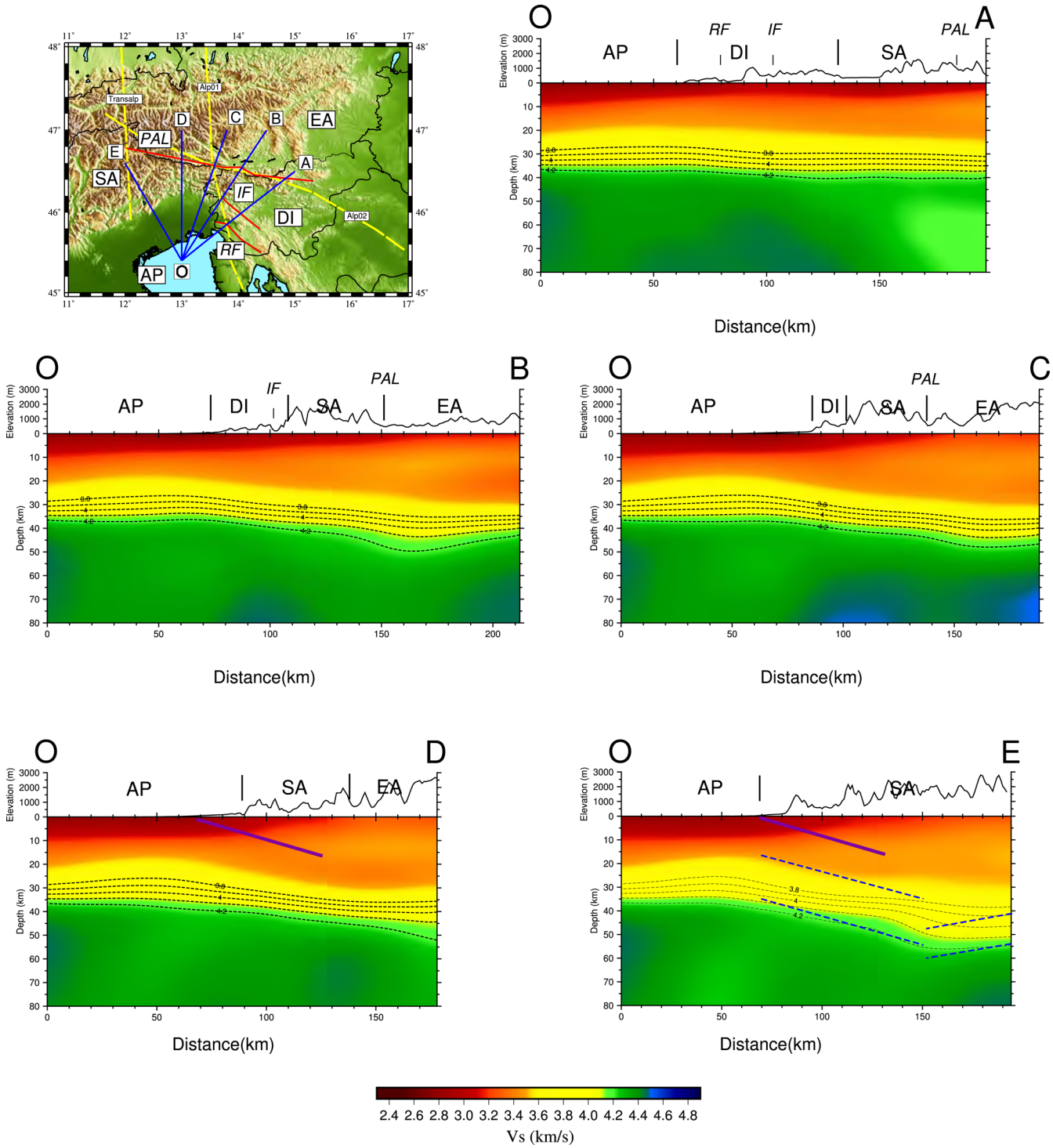

Figure 11. Vertical sections through the 3-D shear wave velocity model along the profiles showed in the map: OA, OB, OC, OD and OE. The black dashed lines show the isolines of velocity from 3.8 to 4.2 km s^{-1}. SA: Southern Alps; PAL: Periadriatic Line; EA: Eastern Alps; IF: Idrjia Fault; RF: Raša Fault; DI: Dinarides; AP: Adriatic Plate and EA: Eastern Alps. The TRANSALP, ALP01 and ALP02 profiles are also plotted (yellow dashed lines). Sections OD and OE: (purple line) sketch of the decollement geometry as inferred by Cheloni *et al*. (2014); (blue dashed line) lower crust boundaries for the TRANSALP profile (TRANSALP Working Group 2002).

has been obtained after an ambient noise tomographic study. Our results provide an unprecedented mapping of the properties of the different lithospheric units.

The surface wave tomographic maps from ambient noise cross-correlation highlight the complex nature of the lithosphere in the region and clearly mark the separation between the Alpine, the Adria and the Dinarides domains. The group velocity anomalies in the period range that sample the upper crust show good quantitative agreement with known geological features, in particular the sedimentary cover in the Po Plain and the periphery of the Pannonian Basin. The Alps are associated with high group velocities at short periods, correspondent to the crystalline basement, and low group

velocities at longer periods, consistent with the presence of thicker crust. Between Italy and Slovenia, the transition between the Alpine and the Dinarides domain is characterized by a complex and composite nature, as showed by surface wave and shear wave velocity maps.

Especially in the Southern Alps, the vertical cross-sections reveal a clear increase of crustal thickness and bending of the crust from east to west, related to the dipping of the Adriatic plate.

A sharp northward dipping of the Moho that coincides at the surface with the leading edge of the Alpine thrust front adjacent to the Friuli Plain in Northeastern Italy mimics fairly well the shallow north-dipping geometry of the decollement inferred from permanent GPS velocity field where high interseismic coupling is reported. From the northern Adriatic domain up to the Idrjia right lateral strike-slip fault system beneath Western Slovenia the crustal thickness is more uniform. Right across Idrjia fault, to the northeast, and along its strike, we report a clear change of the physical properties of the crust up to the uppermost mantle as reflected by the lateral distribution of both group and phase velocity anomalies at relevant periods. Idrjia fault is therefore interpreted as a subvertical fault sampling the whole crust. Our 3-D velocity model favours crustal thickening with Adria underthrusting the Alps at a shallow angle north of the Friuli Plain, where much of the convergence is absorbed and where the destructive 1976 M_s 6.5 thrust Friuli Earthquake sequence took place. In Western Slovenia, the deformation is accommodated by strike-slip motion along the Idrjia strike-slip fault system where the destructive 1511 M_w 6.9 right lateral strike-slip occurred.

ACKNOWLEDGEMENTS

This work is funded by the Generali Group in the framework of The Abdus Salam International Centre for Theoretical Physics-Generali Earthquake Hazard programme and by the Regione Friuli Venezia Giulia, Italy (Cooperazione Internazionale e allo sviluppo). We thank the editors J.C. Afonso, C. Ebinger and M. Behm for useful comments that improved the original manuscript.

REFERENCES

Aoudia, A., 1998. Active faulting and seismological studies for earthquake hazard assessment, *PhD thesis*, University of Trieste, pp. 153.

Aoudia, A., Saraò, A. & Suhadolc, P., 2000. The 1976 Friuli (NE Italy) thrust faulting earthquake: a reappraisal 23 years later, *Geophys. Res. Lett.*, **27**(4), 577–580.

Bajc, J., Aoudia, A., Saraò, A. & Suhadolc, P., 2001. The 1998 Bovec–Krn mountain (Slovenia) earthquake sequence, *Geophys. Res. Lett.*, **28**(9), 1839–1842.

Behm, M., 2009. 3-D modelling of the crustal S-wave velocity structure from active source data: application to the Eastern Alps and the Bohemian Massif, *Geophys. J. Int.*, **179**, 265–278.

Behm, M., Brückl, E., Chwatal, W. & Thybo, H., 2007. Application of stacking and inversion techniques to three-dimensional wide-angle reflection and refraction seismic data of the Eastern Alps, *Geophys. J. Int.*, **170**, 275–298.

Behm, M., Nakata, N. & Bokelmann, G., 2016. Regional ambient noise tomography in the Eastern Alps of Europe, *Pure appl. Geophys.*, **173**, 2813–2840.

Bennet, R.A. *et al.*, 2008. Eocene to present subduction of southern Adria mantle lithosphere beneath the Dinarides, *Geology*, **36**, 3–6.

Bensen, G.D., Ritzwoller, M.H., Barmin, M.P., Levshin, A.L., Lin, F., Moschetti, M.P., Shapiro, N.M. & Yang, Y., 2007. Processing seismic ambient noise data to obtain reliable broad-band surface wave dispersion measurements, *Geophys. J. Int.*, **169**, 1239–1260.

Bleibinhaus, F. & Gebrande, H., 2006. Crustal structure of the Eastern Alps along the TRANSALP profile from wide-angle seismic tomography, *Tectonophysics*, **414**(1–4), 51–69.

Borghi, A., Aoudia, A., Riva, R.E.M & Barzaghi, R., 2009. GPS monitoring and earthquake prediction: a success story towards a useful integration, *Tectonophysics*, **465**, 177–189.

Bragato, P.L. *et al.*, 2014. *The Central and Eastern European Earthquake Research Network-CE3RN*, General Assembly of European Geosciences Union, Wien, Austria, doi:10.13140/RG.2.1.3507.7843.

Bressan, G., De Franco, R. & Gentile, F., 1992. Seismotectonic study of the Friuli (Italy) area based on tomographic inversion and geophysical data, *Tectonophysics*, **207**, 383–400.

Bressan, G., Snidarcig, A. & Venturini, C., 1998. Present state of tectonic stress of the Friuli area (eastern Southern Alps), *Tectonophysics*, **292**, 211–227.

Brückl, E. *et al.*, 2007. Crustal structure due to collisional and escape tectonics in the Eastern Alps region based on profiles Alp01 and Alp02 from the ALP 2002 seismic experiment, *J. geophys. Res.*, **112**, B06308, doi:10.1029/2006JB004687.

Brückl, E., Behm, M., Decker, K., Grad, M., Guterch, A., Keller, G.R. & Thybo, H., 2010. Crustal structure and active tectonics in the Eastern Alps, *Tectonics*, **29**, TC2011, doi:10.1029/2009TC002491.

Caldwell, W.B., Klemperer, S.L., Rai, S.S. & Lawrence, J.F., 2009. Partial melt in the upper-middle crust of the northwest Himalaya revealed by Rayleigh wave dispersion, *Tectonophysics*, **477**(1–2), 58–65.

Castellarin, A., Cantelli, L., Fesce, A.M., Mercier, J., Picotti, V., Pini, G.A., Prossers, G. & Selli, L., 1992. Alpine compressional tectonics in the southern Alps. Relations with the N-Apennines, *Ann. Tect.*, **6**, 62–94.

Castellarin, A. & Cantelli, L., 2000. Neo-Alpine evolution of the Southern Eastern Alps, *J. Geodyn.*, **30**, 251–274.

Castellarin, A., Nicolich, R., Fantoni, R., Cantelli, L., Sella, M. & Selli, L., 2006. Structure of the lithosphere beneath the Eastern Alps (southern sector of the TRANSALP transect), *Tectonophysics*, **414**, 259–282.

Cheloni, D., D'Agostino, N. & Selvaggi, G., 2014. Interseismic coupling, seismic potential and earthquake recurrence on the southern front of the Eastern Alps (NE Italy), *J. geophys. Res.*, **119**, 4448–4468.

Christensen, N.I. & Mooney, W.D., 1995. Seismic velocity structure and composition of the continental crust: a global view, *J. geophys. Res.*, **100**(B7), 9761–9788.

Costa, G., Moratto, L., Suhadolc & P., 2010. The friuliveneziagiulia accelerometric network: RAF, *Bull. Earthq. Eng.*, **8**, 1141–1157.

D'Agostino, N., Avallone, A., Cheloni, D., D'Anastasio, E., Mantenuto, S. & Selvaggi, G, 2008. Active tectonics of the Adriatic region from GPS and earthquake slip vectors, *J. geophys. Res.*, **113**, B12413, doi:10.1029/2008JB005860.

Dal Piaz, G.V., Bistacchi, A. & Massironi, M., 2003. Geological outline of the Alps, *Episodes*, **26**, 175–180.

DeMets, C., Gordon, R.G., Argus, D.F. & Stein, S., 1994. Effect of revisions to the geomagnetic reversal time scale on estimates of current plate motions, *Geophys. Res. Lett.*, **21**, 2191–2194.

Dihel, T., Husen, S., Kissling, E. & Deichmann, N., 2009. High-resolution 3-D P-wave model of the Alpine crust, *Geophys. J. Int.*, **179**, 1133–1147.

Di Stefano, R., Kissling, E., Chiarabba, C., Amato, A. & Giardini, D., 2009. Shallow subduction beneath Italy: three-dimensional images of the Adriatic-European-Tyrrhenian lithosphere system based on high-quality P wave arrival times, *J. geophys. Res.*, **114**, B05305, doi:10.1029/2008JB005641.

Doglioni, C. & Bosellini, A., 1987. Eoalpine and Mesoalpine tectonics in the Southern Alps, *Geol. Rundsch.*, **76**, 735–754.

Doglioni, C. & Carminati, E., 2002. The effects of four subductions in NE Italy: Transalp Conference, *Mem. Sci. Geol.*, **54**, 1–4.

Farina, B.M., 2006. Lithosphere-asthenosphere system in Italy and surrounding areas: optimized non-linear inversion of surface-wave dispersion curves and modelling of gravity bouguer anomalies, *PhD thesis*, University of Trieste.

Fitzko, F., Suhadolc, P., Aoudia, A. & Panza, G.F., 2005. Constraints on the location and mechanism of the 1511 Western-Slovenia earthquake from active tectonics and modeling of macroseismic data, *Tectonophysics*, **404**, 77–90.

Gentile, G.F., Bressan, G., Burlini, L. & De Franco, R., 2000. Three-dimensional V_P and V_P/V_S models of the upper crust in the Friuli area (northeastern Italy), *Geophys. J. Int.*, **141**, 457–478.

Grad, M., Tiira, T. & ESC Working Group, 2009. The Moho depth map of the European Plate, *Geophys. J. Int.*, **176**, 279–292.

Herrmann, R.B., 2013. Computer programs in seismology: an evolving tool for instruction and research, *Seism. Res. Lett.*, **84**, 1081–1088.

Julià, J., Ammon, C.J. & Nyblade, A.A., 2005. Evidence for mafic lower crust in Tanzania, East Africa, from joint inversion of receiver functions and Rayleigh wave dispersion velocities, *Geophys. J. Int.*, **162**, 555–569.

Korbar, T., 2009. Orogenic evolution of the External Dinarides in the NE Adriatic region: a model constrained by tectonostratigraphy of Upper Cretaceous to Paleogene carbonates, *Earth-Sci. Rev.*, **96**(4), 296–312.

Levshin, A.L. & Ritzwoller, M.H., 2001. Automated detection, extraction, and measurement of regional surface waves, *Pure appl. Geophys.*, **158**(8), 1531–1545.

Li, H., Bernardi, F. & Michelini, A., 2010a. Surface wave dispersion measurements from ambient seismic noise analysis in Italy, *Geophys. J. Int*, **180**, 1242–1252.

Li, H., Bernardi, F. & Michelini, A., 2010b. Love wave tomography in Italy from seismic ambient noise, *Earthq. Sci.*, **23**, 487–495.

Lin, F., Moschetti, M.P. & Ritzwoller, M.H., 2008. Surface wave tomography of the western United States from ambient seismic noise: Rayleigh and Love wave phase velocity maps, *Geophys. J. Int.*, **173**, 281–298.

Lippitsch, R., Kissling, E. & Ansorge, J., 2003. Upper mantle structure beneath the Alpine orogen from high-resolution teleseismic tomography, *J. geophys. Res.*, **108**(B8), 2376, doi:10.1029/2002JB002016.

Luo, Y., Yang, Y., Xu, Y., Xu, H., Zhao, K. & Wang, K., 2015. On the limitations of interstation distances in ambient noise tomography, *Geophys. J. Int.*, **201**, 652–661.

Métois, M. *et al.*, 2015. Insights on continental collisional processes from GPS data: dynamics of the peri-Adriatic belts, *J. geophys. Res.*, **120**, 8701–8719.

Michelini, A., Živčić, M. & Suhadolc, P., 1998. Simultaneous inversion for velocity structure and hypocenters in Slovenia, *J. Seimol.*, **2**, 257–265.

Mitterbauer, U. *et al.*, 2011. Shape and origin of the East-Alpine slab constrained by the ALPASS teleseismic model, *Tectonophysics*, **510**, 195–206.

Molinari, I., Argnani, A., Morelli, A. & Basini, P., 2015. Development and testing of a 3D seismic velocity model of the Po Plain sedimentary Basin, Italy, *Bull. seism. Soc. Am.*, **105**, 753–764.

Moulin, A. *et al.*, 2016. The Dinaric fault system: large-scale structure, rates of slip, and Plio-Pleistocene evolution of the transpressive northeastern boundary of the Adriamicroplate, *Tectonics*, **35**, 2258–2292.

Rapine, R., Tilmann, F., West, M. & Ni, J., 2003. Crustal structure of northern and southern Tibet from surface wave dispersion analysis, *J. geophys. Res.*, **108**(B2), 2120, doi:10.1029/2001LB000445.

Sabra, K.G., Gerstoft, P., Roux, P., Kuperman, W.A. & Fehler, M.C., 2005. Surface wave tomography from microseisms in Southern California, *Geophys. Res. Lett.*, **32**, L14311, doi:10.1029/2005GL023155.

Schmid, S.M., Bernoulli, D., Fugenschuh, B., Matenco, L., Schefer, S., Schuster, R., Tischler, M. & Ustaszewski, K., 2008. The Alpine-Carpathian-Dinaridicorogenic system: correlation and evolution of tectonic units, *Swiss J. Geosci.*, **101**, 139–183.

Shapiro, N.M., Campillo, M., Stehly, L. & Ritzwoller, M.H., 2005. High-resolution surface-wave tomography from ambient seismic noise, *Science*, **307**, 1615–1618.

Stehly, L., Campillo, M. & Shapiro, N.M., 2006. A study of the seismic noise from its long range correlation properties, *J. geophys. Res.*, **111**, doi:10.1029/2005JB004237.

Stipčević, J., Tkalčić, H., Herak, M., Markušič, S. & Herak, D., 2011. Crustal and uppermost mantle structure beneath the External Dinarides, Croatia, determined from teleseismic receiver functions, *Geophys. J. Int.*, **185**, 1103–1119.

Šumanovac, F. & Dudjak, D., 2016. Descending lithosphere slab beneath the Northwest Dinarides from teleseismic tomography, *J. Geodyn.*, **102**, 171–184.

Swiss Seismological Service (SED) at ETH Zurich, 2015. *The Site Characterization Database for Seismic Stations in Switzerland,* Federal Institute of Technology, Zurich, doi:10.12686/sed-stationcharacterizationdb (retrieved 28 September 2017 from http://stations.seismo.ethz.ch).

Tesauro, M., Kaban, M.K. & Cloetingh, S.A.P.L., 2008. EuCRUST-07: a new reference model for the European crust, *Geophys. Res. Lett.*, **35**, L05313, doi:10.1029/2007GL032244.

TRANSALP Working Group, 2002. First deep seismic images of the Eastern Alps reveal giant crustal wedges and transcrustal ramps, *Geophys. Res. Lett.*, **29**(10), 92-1–92-4.

Vosteen, H.D., Rath, V., Clauser, C. & Lammerer, B., 2003. The thermal regime of the Eastern Alps from inversion analyses along the TRANSALP profile, *Phys. Chem. Earth*, **28**, 393–405.

Yang, Y. & Ritzwoller, M.H., 2008. Characteristics of ambient seismic noise as a source for surface wave tomography, *Geochem. Geophys. Geosyst.*, **9**, Q02008, doi:10.1029/2007GC001814.

Yanovskaja, T.B. & Ditmar, P.G., 1990. Smoothness criteria in surface wave tomography, *Geophys. J. Int.*, **102**, 63–72.

Yanovskaya, T.B., 1997. Resolution estimation in the problems of seismic ray tomography, Izvestia, *Phys. Solid Earth*, **33**(9), 762–765.

Yanovskaya, T.B., Kizima, E.S. & Antonova, L.M., 1998. Structure of the crust in the Black Sea and adjoining regions from surface wave data, *J. Seismol.*, **2**, 303–316.